

Electronic Supplementary Information for

Super-Resolution Optofluidic Scanning Microscopy

Biagio Mandracchia,¹ Jeonghwan Son,¹ and Shu Jia^{1,*}

¹ Wallace H. Coulter Department of Biomedical Engineering, Georgia Institute of Technology and Emory University, Atlanta, GA, USA

* Corresponding author: shu.jia@gatech.edu

Experimental Setup.

To excite fluorescence, we used two lasers: a 120-mW, 647-nm laser (Coherent, OBIS 647 nm LX 120 mW) and a 150-mW, 488-nm laser (Coherent, OBIS 488 nm LX 100 mW). The beams were expanded 10× with a beam expander constructed from two achromatic lenses of focal length $f_1 = 25$ mm and $f_2 = 250$ mm, respectively. A pinhole was placed at the focal plane between the two achromatic lenses to obtain a more uniform beam profile. The collimated beam exiting from the beam expander passed through a microlens array (MLA-S100-f4-A-R1, RPC Photonics), which generated a grid of focal spots. A relay lens placed at the back port of the microscope (Ti-U, Nikon) formed an image of the grid in correspondence of the focal plane of the objective lens (NA 1.45, CFI Plan Apochromat Lambda 100× Oil, Nikon). This generated another grid of diffraction-limited spots at the sample plane. The fluorescence emission was collected by the objective, passed through a dichroic mirror (Chroma) and a tube lens, and finally detected by a sCMOS camera (Hamamatsu ORCA 4.0 V3) mounted on the microscope (**Figs. 1a** and **S1**).

To achieve a near diffraction-limited performance of the wide-field epifluorescence system, we projected the excitation pattern onto a calibration slide made by a uniform solution of fluorescent dyes (Alexa Fluor 647 and Alexa Fluor 488). Then, we translated the microlens array along the optical axis until the apparent size of each fluorescent spot is minimized.

Optofluidic measurements were performed while introducing the samples through plastic microfluidic channels with a glass bottom. The dimensions of the microfluidic channel were 58.5 mm × 1 mm × 200 μm (Fluidic 138, Chipshop). The flow was controlled by a pressure pump (Mk III, Elveflow) and a flow sensor (Elveflow) was used as a feedback loop. The feedback loop maintained the average flow speed at 19.5 μm/s for a constant displacement of the sample at 97.5 ± 1.4 nm/frame (**Fig. S2**). Notably, the flow has been maintained stable enough to guarantee that the sample displacement between the two consecutive frames is comparable with the size of the digital pinhole (in our case 97.5 nm). In case of any flow fluctuations, image stabilization as to precisely track the microfluidic motion of the samples frame-by-frame is a critical step in the OSM reconstruction. The work utilizes image correlation, and to enhance the tracking, we can use fiducial markers in the flow to correct the drift for an optimum image stabilization (with <100 nm alignment precision) of the specimens. The camera frame rate was set to 200 Hz using a segmented sensor chip.

The microscope system was equipped with an automated X-Y stage (Prior). A custom μManager script [1] was written to synchronize the stage and the camera for the acquisition of stage-scanned images. The translation step of the stage was set to 98 nm in order to keep the displacement between frames close to the value of optofluidic measurements. We acquired the images of both the 100-nm TetraSpeck™ beads and the fluorescent-labeled microtubules using the full sensor chip and the camera frame rate was set to 50 and 100 Hz, respectively.

Calibration.

The OSM configuration utilizing fluidic scanning allows for a simplified optical setup (**Fig. S3**). For the optimum performance, it requires prior calibration steps as in other similar image scanning microscopy (ISM) implementations. First, it is critical to precisely identify the position of each illumination spot across the field of view (FOV). We performed this measurement by recording a set of images from a slide containing a uniform concentration of fluorophores. The images acquired were averaged and the positions of the foci were determined by peak detection. It is also feasible to perform such an operation by Fourier analysis [1]. However, we verified peak detection to be more accurate (**Fig. S4**). Second, a super-resolution image was reconstructed by utilizing the image sequence of the same object recorded as it was continuously translated into different regions of the FOV. Therefore, each image of the sequence varies in background intensity, which was calibrated and removed in post-processing. Such variation can be further avoided using strategies for uniform illumination [2]. Finally, it is important to notice that during the first calibration step it is necessary to check for potential optical aberrations caused by the glass/fluid interface. If this is the case, the position of the imaging plane should be changed.

Sample preparation.

To prepare fluorescent beads for calibration and resolution measurement, we used 4- μm and 100-nm TetraSpeck™ microspheres (T7283 & T7279, Invitrogen), respectively. The 4- μm beads were diluted in PBS and flown through the microfluidic channel. The 100-nm beads were directly dispersed on a glass slide to form beads aggregates.

A prepared slide of fluorescent-labeled microtubules in bovine pulmonary artery endothelial (BPAE) cells (F14781, ThermoFisher) was used for resolution assessment. Microtubules were stained with green-fluorescent BODIPY FL goat anti-mouse IgG (emission max: 513 nm). Another slide of fixed fluorescent-labeled microtubules of COS-7 cells were prepared by immunostaining with beta Tubulin Monoclonal Antibody (#32-2600, ThermoFisher) and Goat anti-Mouse IgG (H+L) Highly Cross-Absorbed Secondary Antibody, Alexa Fluor Plus 647 (#A32728, ThermoFisher) as Primary 1:100 (1.5 $\mu\text{g}/\text{ml}$) and Secondary 1:1000 optimized concentration. The COS-7 cells were permeabilized by 4% Paraformaldehyde fixative solution for 12 minutes. After washing several times with the prepared rinse buffer (50 ml of PBS, 0.25 ml of NGS, and 250 μl of Triton x-100), the block buffer (10 ml of PBS, 0.5 ml of NGS, 0.1 g of BSA, and 50 μl of Triton x-100) were prepared. Next, the permeabilization buffer (5 ml of blocking buffer and 100 μl of Triton x-100) were applied for 30 minutes. Then, cells were prepared to be immunolabeled after washing several times with rinse buffer. The primary labeling solution was applied for 3 hours under no exposure of light. The secondary labeling solution was then applied for 1 hour after washing primary solution. After final washing, the immune-stained cells in beta Tubulin were prepared in 3.5 cm cell plate.

For fluorescent stained cells in flow, we first prepared 90% confluency of COS-7 cells growing on a 10 cm plate well plate. All fluorescent staining stocks were prepared according to proper protocols provided by distributor (Invitrogen). After washing once with HBSS (Hanks' Balanced Salt Solution, Invitrogen), different amounts of staining solutions were applied with complete DMEM (Dulbecco's Modification of Eagle's Medium, Invitrogen). For MitoTracker™ Green FM probes (M7514, Invitrogen), 4 μl from 200 nM working solution was treated with 10 mL of complete DMEM for 45 minutes. For CellMask™ Deep Red plasma membrane stain (C10046, Invitrogen), 1 \times working solution with 10 ml of DMEM was treated for 15 minutes. After incubation, we washed twice with HBSS to refrain from overloading. Next, 3 ml of Trypsin was applied for 40 seconds then aspirated and incubated for 5 minutes inside incubator maintaining at 37°C and 5% CO_2 level.

To maintain favorable conditions for live cells during visualization, we diluted it with 6 ml of Opti-MEM™ (ThermoFisher Scientific) and split cell mixtures into three of 2 ml vials for multiple experiment trials. All stained cells were prepared right before visualization.

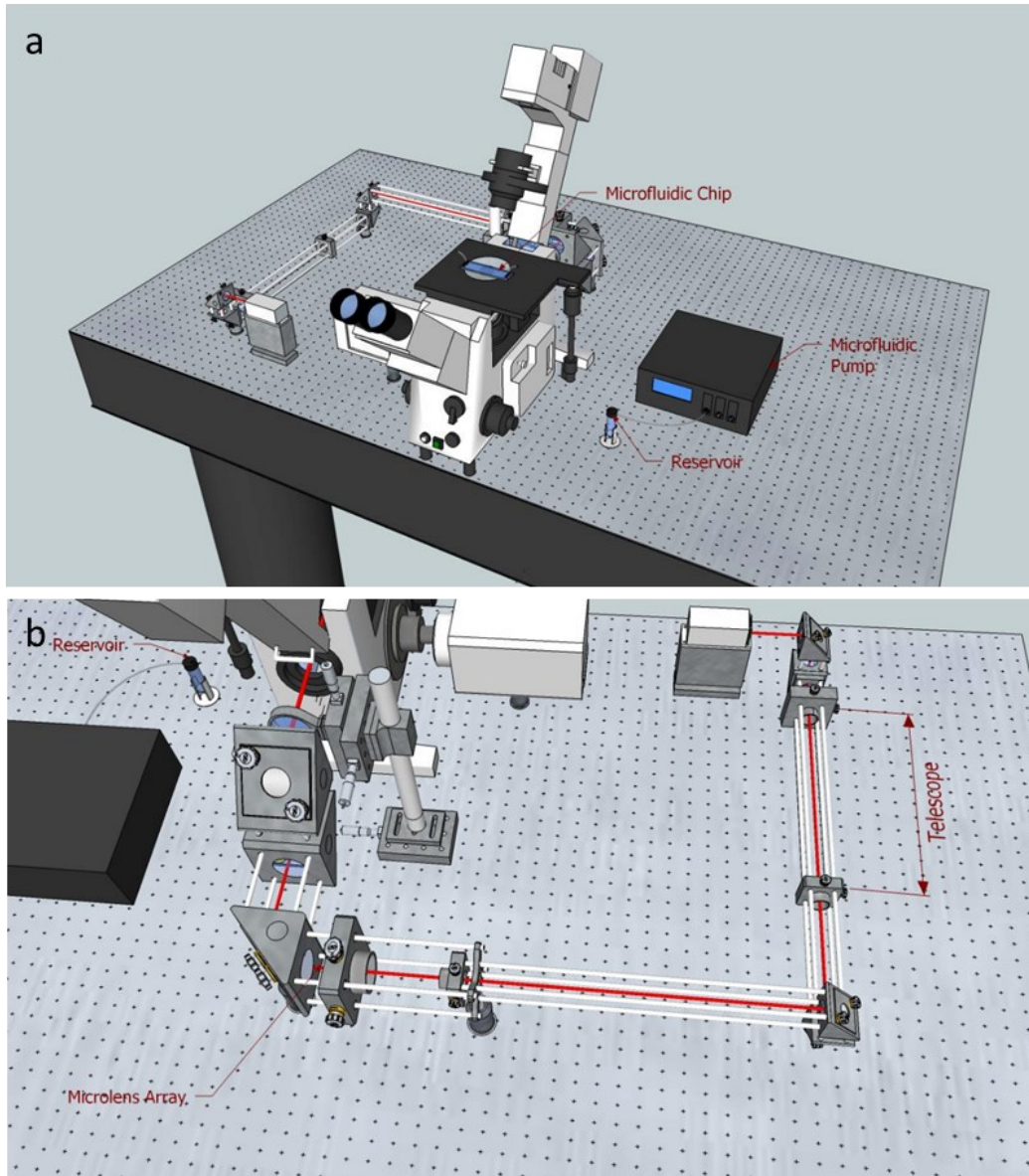


Figure S1: Experimental setup. (a) Front view of the OSM experimental setup. The microfluidic chip was placed on an inverted microscope and connected to a pressure pump. (b) The illumination light exiting the solid-state laser was expanded using a couple of achromatic lenses in order to fill the back-focal plane of the microlens array. Then, the focal plane of the microlens array was imaged at the back-focal plane of the microscope objective by a relay lens placed at the back-port of the microscope.

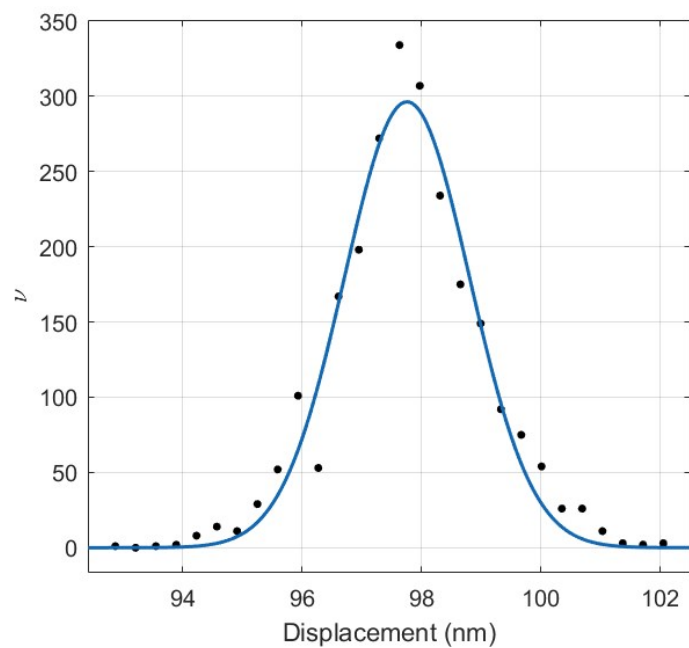


Figure S2: Flow stability and sample displacement per frame. Fluctuations in the flow rate affect the precision of the flow direction. We used a flow rate sensor to stabilize the flow and control the sample displacement during image acquisition. Here, we report a histogram of the flow rate in term of displacement per frame. The Gaussian fitting of the histogram yields an average displacement at 97.5 nm/frame with an uncertainty of 1.4 nm/frame, which is well below the pixel size in the super-resolution image (32.5 nm).

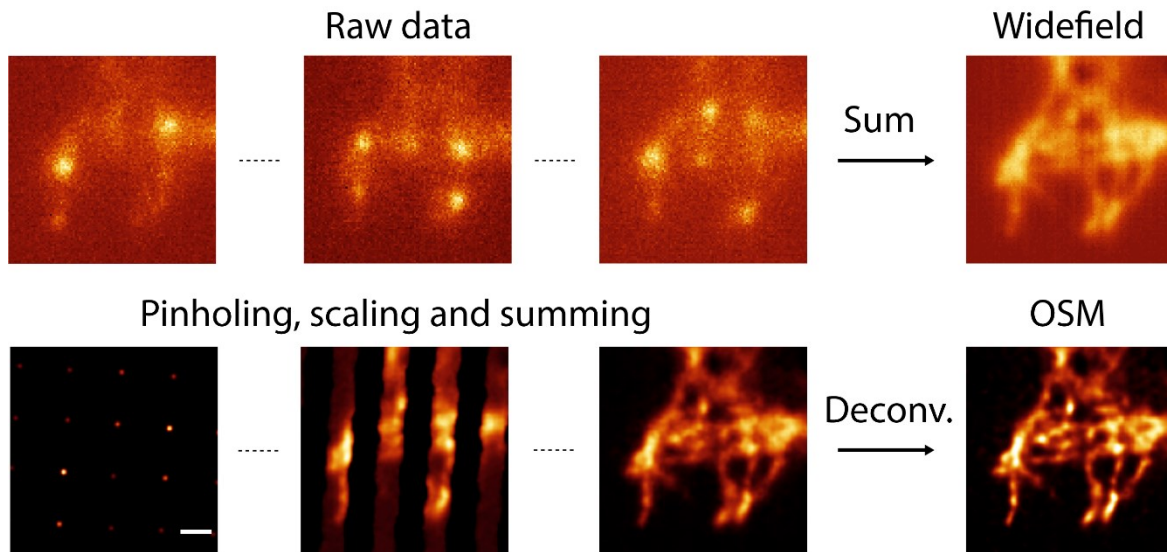


Figure S3: Image reconstruction in optofluidic scanning microscopy. A COS-7 cell immune-stained on microtubules scans through a fixed array of diffraction-limited spots. A region of interest is selected, tracked and aligned using cross-correlation (raw data). A pinhole mask is applied to each frame, which is then scaled to perform pixel reassignment. The sum of these frames has both a higher signal-to-background ratio and improved resolution ($\sqrt{2}\times$). Finally, deconvolution is applied in order to obtain the full resolution enhancement ($2\times$) in the OSM image. The wide-field image is obtained by summing the raw frames.

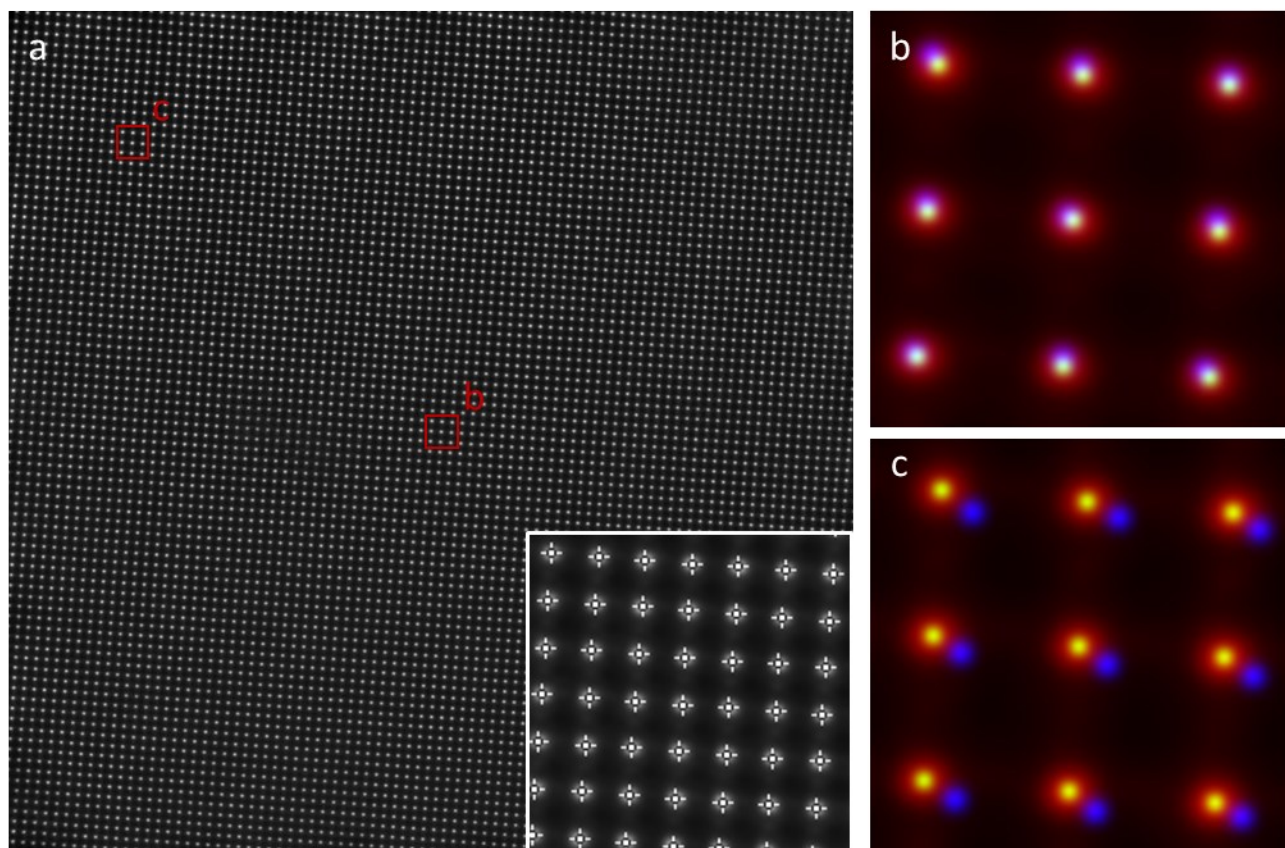


Figure S4: Calibration of the foci positions. (a) We calibrated the position of the focal spots generated on the sample plane by using a slide containing a uniform distribution of fluorescent dyes. We acquired a sequence of several images of the fluorescent dye and averaged it in order to reduce noise. Then, we generated a map of the focal spots by evaluating the position of the local maxima in the image (a, inset). (b, c) We compared this map (green channel) with another one generated by Fourier analysis (blue channel) to evaluate which offers a more reliable estimation of the original positions (red channel). We observed that the green channel provides a reliable estimation across FOV (optimum overlap in both the center of the image (b) and toward the edge of the FOV (c)). In contrast, the blue channel exhibited slight deviations from the original positions already at the center of the image (b), which became severe toward the edge of the FOV (c).

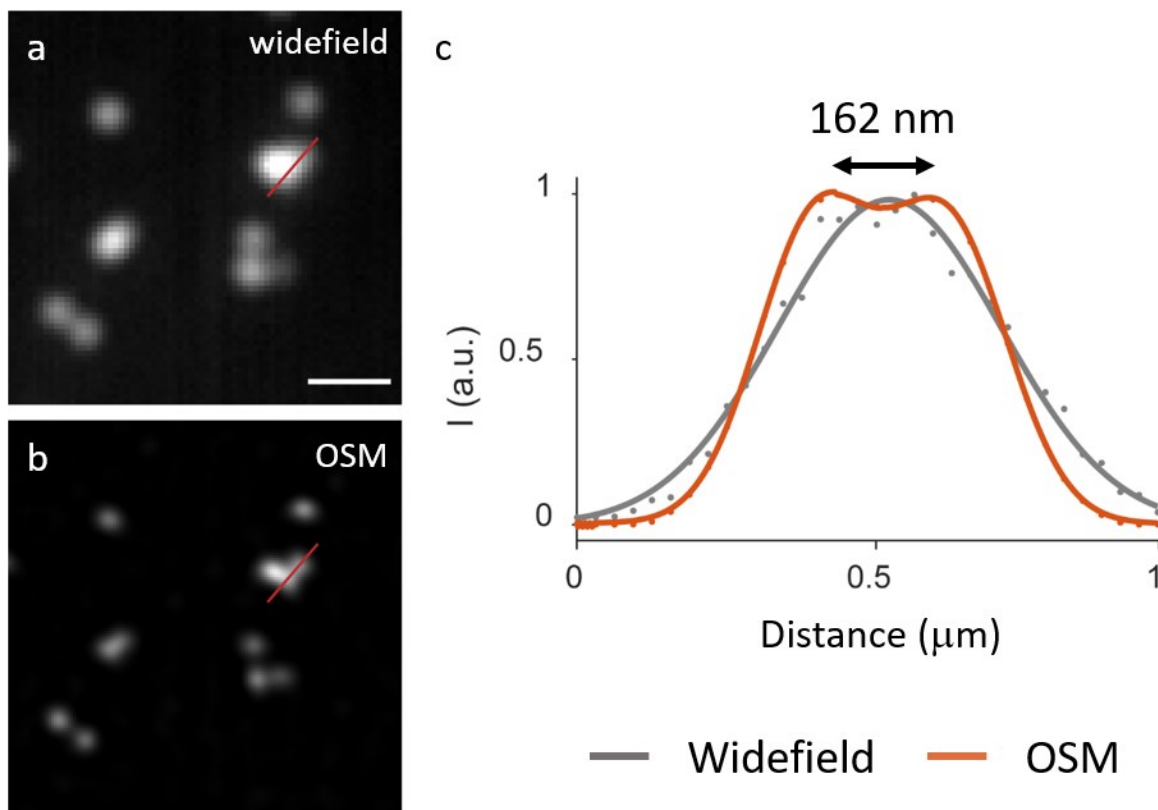


Figure S5: Evaluation of the resolution using fluorescent beads. (a,b) Wide-field (a) and OSM (b) image of fluorescent beads emitting in the dark red ($\lambda_{\text{em}} = 680 \text{ nm}$). (c) Cross-sectional profiles corresponding to the red lines in (a), gray dots, and (b), red dots. The gray and red solid lines were obtained by Gaussian fitting of the gray and red dots, respectively. In both cases, the experimental data were fitted using two Gaussian terms. Two beads separated 162 nm apart can be well resolved using OSM, 1.9 \times improvement over the diffraction limit.

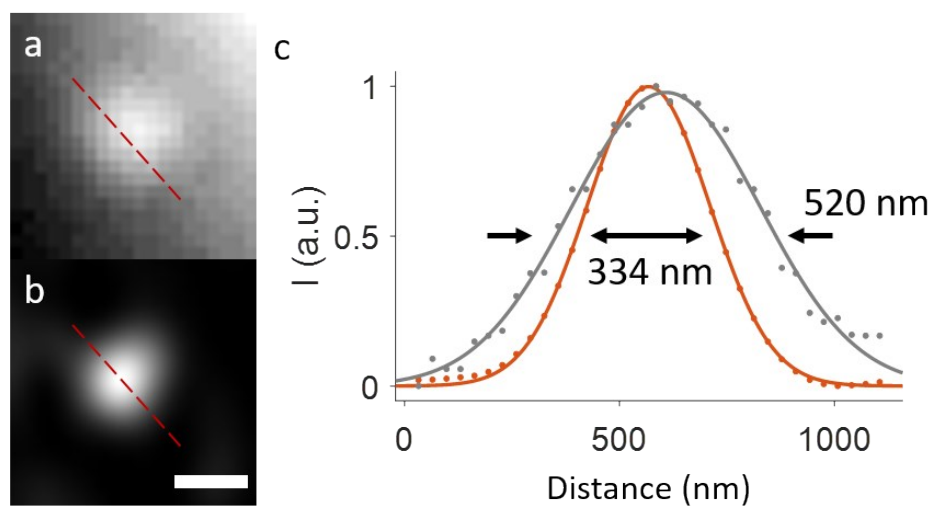


Figure S6: (a,b) Same wide-field (a) and OSM (b) images of the membrane vesicle as displayed in **Fig. 4t** and **4u** in the main text. (c) Cross-sectional profiles corresponding to the dashed lines in (a), gray line, and (b), red line. Indicated by the arrows, the full-width half-maximum (FWHM) values of both profiles measured by Gaussian fitting show a >100-nm enhancement in resolution between wide-field microscopy and OSM. Scale bar: 500 nm.

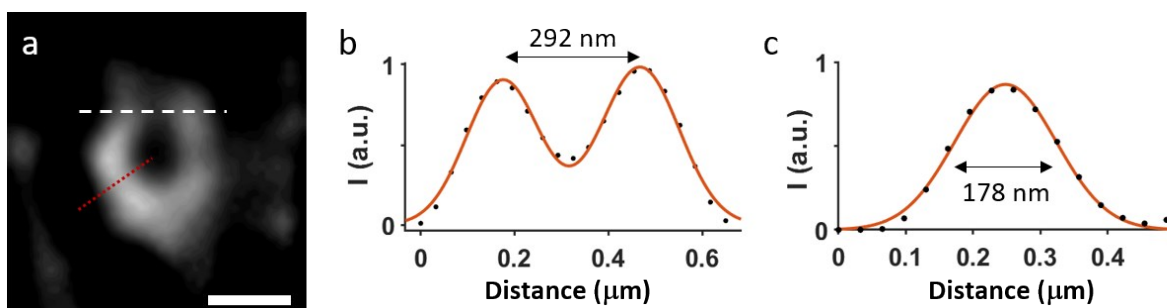


Figure S7: (a) Same OSM image of the membrane vesicle as displayed in **Fig. 4w** in the main text. (b) Cross-sectional profile corresponding to the dashed white line in (a). (c) Cross-sectional profile corresponding to the dotted red line in (a). (b,c) show a significant improvement in resolution of fine structures below the diffraction limit using OSM. Scale bar: 400 nm.

	iSIM [4] (widefield)	iSIM [4] (MPSS)	iSIM [4] (decon.)	OSM (widefield)	OSM (MPSS)	OSM (decon.)	OSM (widefield)	OSM (MPSS)	OSM (decon.)
NA	1.45	1.45	1.45	1.45	1.45	1.45	1.45	1.45	1.45
λ_{em}	605 (red)	605 (red)	605 (red)	680 (dark red)	680 (dark red)	680 (dark red)	515 (green)	515 (green)	515 (green)
Expected FWHM*	273 nm	193 nm	136 nm	303 nm	214 nm	151 nm	237 nm	167 nm	118 nm
Lateral resolution	281 ± 11 nm	213 ± 26 nm	145 ± 14 nm	314 ± 16 nm	222 ± 17 nm	165 ± 6 nm	241 ± 30 nm	190 ± 36 nm	122 ± 8 nm
Resolution improvement		1.3 ± 0.2	1.9 ± 0.2		1.4 ± 0.1	1.9 ± 0.1		1.3 ± 0.2	2.0 ± 0.2

Table S1: Resolution improvement in OSM images. As a reference, we provide the resolution improvement measured for iSIM previously reported in [4]. For both OSM and iSIM, all numbers were derived as the average of the apparent width of 10 sub-diffractive beads of 100-nm diameter. It can be observed the resolution improvement for OSM after deconvolution is consistent with resolution doubling. For easy comparison, we used the same terms reported in iSIM: MPSS, the intermediate image (or the INT image as in Fig. 2 in the main text) obtained after multifocal-excitation, pinholing, scaling and summing. Decon.: final result obtained by deconvolving the MPSS image.

Microscope Technique	Spatial Resolution	Detection objective	Samples
Lens free [6-7]	n/a	n/a	Microparticles, White blood cells
LSM [8-10]	n/a (transverse), 4.6-7.5 μm (axial)	40x, 0.75 NA	Membrane vesicles
	$\sim 0.8 \mu\text{m}$ (transverse), $\sim 10 \mu\text{m}$ (axial)	20x, 0.45 NA	Tumor spheroids
	$\sim 0.51 \mu\text{m}$ (transverse), $\sim 2.1 \mu\text{m}$ (axial)	60x, 1.10 NA	Mouse breast cancer cells
VIFFI [11]	$\sim 700 \text{ nm}$	20x, 0.75 NA	Jurkat cells <i>C. Reinhardtii</i> cells <i>E. gracilis</i> cells
FOFM [12]	1 μm (demonstrated), 0.6 μm (theoretical limit)	n/a (Fresnel lenses embedded on chip)	HeLa cells
SLM [13]	$\sim 160 \text{ nm}$ (localization accuracy)	60x, 0.9 NA	Jurkat cells

Table S2: Optofluidic fluorescence microscopy techniques. We provide a summary of selective optofluidic techniques for fluorescence imaging. LSM: light-sheet microscopy. VIFFI: virtual-freezing fluorescence imaging. FOFM: fluorescence optofluidic microscope. SLM: single-molecule localization microscopy. An in-depth review of current optofluidic microscopy (including label-free imaging techniques) is presented in Ref. [5].

Supplementary References

1. A. Edelstein, N. Amodaj, K. Hoover, R. Vale, and N. Stuurman, *Current Protocols in Molecular Biology*, pp. 1–17, (2010).
2. F. Ströhl and C. F. Kaminski, *Methods Appl. Fluoresc.* **3**, 14002 (2015).
3. R. Voelkel and K. J. Weible, *Opt. Fabr. Testing, Metrol. III* **7102**, 71020J (2008).
4. A. G. York, P. Chandris, D. D. Nogare, J. Head, P. Wawrzusin, R. S. Fischer, A. Chitnis, and H. Shroff, *Nat. Methods* **10**, 1122 (2013).
5. P. Paiè, R. Martínez Vázquez, R. Osellame, F. Bragheri and A. Bassi, *Cytom. Part A*, **93**, 987–996 (2018).
6. Coskun AF, Su TW, Ozcan A. *Lab Chip*, **10**, 824–827 (2010).
7. Coskun AF, Sencan I, Su TW, Ozcan A. Wide-field lensless fluorescent microscopy using a tapered fiber-optic faceplate on a chip. *Analyst*, **136**, 3512–3518 (2011).
8. Deschout H, Raemdonck K, Stremersch S, Maoddi P, Mernier G, Renaud P, Jiguet S, Hendrix A, Bracke M, Van den Broecke R, et al., *Nanoscale*, **6**, 1741–1747 (2014).
9. Paiè P, Bragheri F, Bassi A, Osellame R., *Lab Chip*, **16**, 1556–1560, (2016).
10. F. Sala, M. Castriotta, P. Paiè, A. Farina, S. D Annunzio, A. Zippo, R. Osellame, F. Bragheri and A. Bassi, *Biomed. Opt. Express*, **11**, 4397–4407 (2020).
11. H. Mikami, M. Kawaguchi, C. J. Huang, H. Matsumura, T. Sugimura, K. Huang, C. Lei, S. Ueno, T. Miura, T. Ito, K. Nagasawa, T. Maeno, H. Watarai, M. Yamagishi, S. Uemura, S. Ohnuki, Y. Ohya, H. Kurokawa, S. Matsusaka, C. W. Sun, Y. Ozeki and K. Goda, *Nat. Commun.*, **11**, 1–11, (2020).
12. Pang S, Han C, Lee LM, Yang C., *Lab Chip*, **11**, 3698–3702 (2011).
13. L. E. Weiss, Y. Shalev Ezra, S. Goldberg, B. Ferdman, O. Adir, A. Schroeder, O. Alalouf and Y. Shechtman, *Nat. Nanotechnol.*, **15**, 500–506 (2020).